Int. J. Nano Dimens., 12 (3): 222-238, Summer 2021

ORIGINAL ARTICLE

# Experimental and theoretical electronic absorption pectra, optical, photoelectrical characterizations of 1, 2, 3-Thiazaphosphinine and 1, 2-Azaphospholes bearing a chromone ring: Solvatochromic effect and TD/DFT approach

***Shimaa Abdel Halim Hussein*** [1,*]***, Tarik E. Ali*** [1,2]

[1] *Department of Chemistry, Faculty of Education, Ain Shams University, Roxy, 11711, Cairo, Egypt*
[2] *Department of Chemistry, Faculty of Science, King Khalid University, Abha, Saudi Arabia*

Received 27 January 2021; revised 10 March 2021; accepted 03 April 2021; available online 10 April 2021

**Abstract**

Geometry, global energetic and dipole moment of the studied structures **1-4** in the ground state are calculated using the DFT/B3LYB/6-311++G (d,p) level of theory. It has been uncovered that compounds containing 1, 2, 3-thiazaphosphinine and 1, 2-azaphospholes bearing a Chromone ring structure displays noteworthy biological properties. The studied compounds **1-4** are non-planar, as indicated from the dihedral angles. Using frontier molecular orbital (FMO) analysis, various spectroscopic and quantum chemical parameters are evaluated. Besides, absorption energies, oscillator strength, and electronic transitions of 1, 2, 3-thiazaphosphinine and 1, 2-azaphospholes **1-4** molecules have been derived at TD-DFT/CAM-B3LYP/6-311++G (d, p) computations utilizing a PCM and measured in different solvents polar and non-polar experimentally in Uv-Vis spectra. The second-order perturbation interactions between donor and acceptor MOs of the ground state and the natural bond orbital (NBO) analysis show a localization and delocalization of electron density, intermolecular Charge Transfer CT character of n-π*, π-π* transitions. The calculated at the same level of theory which NLO, α, Δα and first order β were showed promising optical properties. For the understanding of reactivity points, the molecular electrostatic potential surfaces (MEPS) plots have been computed. All the calculations have been performed in the gas phase.

**Keywords:** *DFT/TD-DFT/ B3LYB/6-311++G (d, p), MEPS, NLO and NBO Analysis, Optoelectronic Application, Uv-Vis Spectra, 1, 2, 3-Thiazaphosphinine, 1, 2-Azaphospholes.*

**How to cite this article**

*Abdel Halim Hussein Sh., Ali T.E. Experimental and theoretical electronic absorption spectra, optical, photoelectrical characterizations of 1, 2, 3-Thiazaphosphinine and 1, 2-Azaphospholes bearing a chromone ring: Solvatochromic effect and TD/DFT approach. Int. J. Nano Dimens., 2021; 12(3): 222-238.*

## INTRODUCTION

1, 2, 3-thiazaphosphinine and 1, 2-azaphospholes are important class of Phosphonates and organ phosphorus family in recent years due to their biological properties [1,2]. They are considered as antiproliferative [3], enzyme inhibitory [4], antibiotic [5], analgesic [6], and as promising anticancer therapeutic drugs [7]. On the other hand, chromone compounds are well known natural and synthetic products showed significant biological activities including antiplatelet [8], antiallergic [9], antiangiogenic [10], antirheumatic [11], antitumor [12], neuroprotective [13], HIV-inhibitory [14,15], antimicrobial [16,17], antioxidant [18], and anti-inflammatory [19]. Appropriately, it seems, by all accounts, to be exceedingly appealing to study the previously synthesized 1, 2, 3-thiazaphosphinine and 1, 2-azaphospholes bearing a chromone ring **2-4** [20] of biological intrigue from computational investigation point of view. Density functional theory-based computational study plays a vital

* Corresponding Author Email: *Shimaabdelhalim@edu.asu.edu.eg*

role in calculating the electronic structure of molecular systems and identifying the new drug candidates. The DFT method favorite the accuracy and checking the experimental values of molecular geometry, vibrational frequencies, atomic charges, dipole moment, thermodynamically properties, etc [21-24].

There is no reported systematic study on the UV-Vis spectra of 1, 2, 3-thiazaphosphinine and 1, 2-azaphospholes bearing a chromone ring. Thus, the present work attempts to provide a comprehensive study of experimental UV-Vis spectra for these compounds using Time-dependent density functional theory (TD-DFT) calculations at CAM-B3LYP/6-311++G (d, p). Also, the contributing configurations and MOs are characterized by the origin of each absorption band. The charge transfer of the electron density in the studied compounds is characterized by natural bond orbital analysis (NBO). Due to theoretical chemistry, it has become possible to anticipate many physical and chemical properties of molecules. In the current examination, using DFT calculations, structural entities, chemical reactivity parameters, spectroscopic data, some global reactivity descriptors have been explored. The spectrophotometric measurements of elucidating the optical constants of the prepared compounds **1-4** are investigated in a wide range of spectra.

## EXPERIMENTAL

*The studied compounds*

The studied compounds were prepared in our laboratory and reported in the literature [20]. The proposed compounds **1–4** are shown in **Figure 1**. They are 2-cyano-3-(4-oxo-4*H*-chromone-3-yl)prop-2-enamide (**1**), 2-hydroxy-2-oxido-3-(4-oxo-4H-chromen-3-yl)-1,2-dihydro-5H-1,2-azaphosphol-5-one (**2**), 2-ethoxy-6-(4-oxo-4H-chromen-3-yl)-2-sulfido-2, 3-dihydro-4H-1, 3, 2-thiazaphosphinin-4-one (**3**) and 2-hydroxy-3-imino-4-[(4-oxo-4H-chromen-3-yl)methylidene]-2-oxido-1, 2-azaphospholidin-5-one (**4**).

*Solvents*

Polar (methanol and butanol) and non-polar (dioxane and toluene) solvents were obtained from Merck, AR- grade, and were used without further purification.

*Apparatus*

A Perkin Elmer lambda 4B spectrophotometer using 1.0 cm fused quartz cells were used to measure the electronic absorption spectra over the range 200-900 nm. Spectral analysis of transmittance and reflectance are performed in the wavelength range of 200-750 nm.

*Computational details*

Khon-Sham's (DFT) calculations were performed on an Intel (R) Core (TM) i7 computer using the Gaussian-09 program package without any constraint on the geometry [25]. The geometry of the molecules studied in this is optimized by DFT/B3LYP method using the 6-311++G (d, p) basis set [26-28]. The FMO analysis and quantum chemical study has been performed using Gauss View 5.0.9 [29] or chem craft 1.6 [30] software packages. Also, the following equations [31-33], were calculated the total static dipole moment ($\mu$), $\langle\Delta\alpha\rangle$, and $\langle\beta\rangle$, values.

$$\mu = (\mu^2_x + \mu^2_y + \mu^2_z)^{1/2},$$
$$\langle\alpha\rangle = 1/3\,(\alpha_{xx} + \alpha_{yy} + \alpha_{zz}),$$
$$\Delta\alpha = ((\alpha_{xx} - \alpha_{yy})^2 + (\alpha_{yy} - \alpha_{zz})^2 + (\alpha_{zz} - \alpha_{xx})^2/2)^{1/2},$$
$$\langle\beta\rangle = (\beta^2_x + \beta^2_y + \beta^2_z)^{1/2}, \quad (1)$$

Where

$$\beta_x = \beta_{xxx} + \beta_{xyy} + \beta_{xzz},$$
$$\beta_y = \beta_{yyy} + \beta_{xxy} + \beta_{yzz},$$
$$\beta_z = \beta_{zzz} + \beta_{xxz} + \beta_{yyz}. \quad (2)$$

Using the predicted energies of HOMO and LUMO, global reactivity descriptors were calculated as follows: $\chi$= ($I$+ $A$)/2 (electronegativity), $\eta$= ($I$−$A$)/2 (chemical hardness), $S$= 1/2$\eta$ (global softness), ω =$\mu^2$/2$\eta$ (electrophilicity) where $I$ and $A$ were ionization potential and electron affinity, and $I$= $-E_{\text{HOMO}}$ and $A$=$-E_{\text{LUMO}}$, respectively [34, 35]. Absorption energies (λ in nm), Oscillator strength (ƒ), and Transitions of all compounds **1–4** have been calculated at TD- CAM -B3LYP/6-311++G (d, p) level of theory [36, 37].

The natural bond orbital method (NBO) [38] used to investigate the reactive sites of the compounds **1–4**, the molecular electrostatic potential (MEP) was computed, the donor-acceptor interactions were used to evaluate the second order Fock matrix [39]. For each donor (*i*) and acceptor (*j*), the stabilization energy E $^{(2)}$ associated with the delocalization $i \rightarrow j$ was estimated as:

$$E^{(2)} = \Delta E_{ij} = q_i\,(F\,(ij)^2/\varepsilon_j - \varepsilon_i), \quad (3)$$

Where $q_i$ is the donor orbital occupancy,

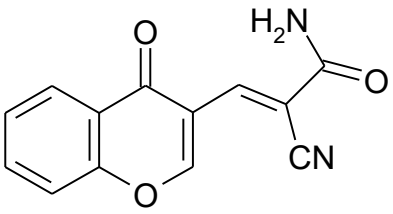


**1**

Compound **1**

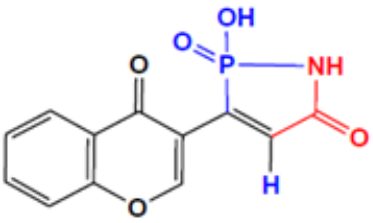


Compound **2**

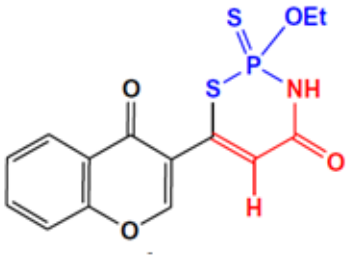


Compound **3**

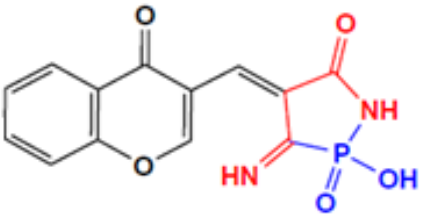


Compound **4**

Fig. 1. The proposed compounds 1–4.

$\varepsilon_i$ and $\varepsilon_j$ are diagonal elements and $F(ij)$ is the off-diagonal NBO Fock matrix element. For the conversion factors of $\alpha$, $\beta$, and HOMO and LUMO energies in atomic and cgs units: 1 atomic unit (a.u.) = 0.1482 × $10^{-24}$ electrostatic unit (esu) for polarizability $\langle\alpha\rangle$, 1 a.u. = 8.6393×$10^{-33}$ esu for first hyperpolarizability $\langle\beta\rangle$.

## RESULT AND DISCUSSION

*Electronic structures*

*Geometry, Ground state properties and Global reactivity descriptors*

In the present study all compounds **1–4** Fig. 2 have been studied to determine various structural and chemical parameters using density functional theory DFT/B3LYB at 6-311++G (d, p) basis set. The optimized geometrical parameters (bond lengths and bond angles) were shown in Figs. 3 and 4. All compounds **1–4** is having C1 point group symmetry as predicted by DFT investigation. The frontier molecular orbital's (FMO) of previously synthesized compounds **1–4** is presented in Figs. 5 & 6; the electronic parameters and the global reactivity descriptors' statistics are given in Table 3. Also, the dihedral angles and natural charge of the studied compounds **1-4** were listed in Tables 1 and 2.

The studied compounds **1-4** all calculated bond lengths were in the range from 1.387 to 1.509 Å in the chromone moiety (c.f. Fig. 3). These were overestimated than the experimental values in literature by 1%, (c.f. Refs 40 & 41), whereas the computed C-P and C-S bond lengths are overestimated than the experimental values by 4%. At the same time, the C-C bond lengths for compounds **1-4** (1.449-1.479Å) were found to be like the central bond in butadiene (1.463Å) [40], while the C=C bond lengths (1.387-1.390Å) did not differ very much from the C=C bond length in ethylene [41]. These conclusions were suggested by the considerably large O-C bond lengths and shorten C=O bond length. The small difference between calculated and observed bond lengths indicated the power of the method used in the calculation which was carried out in the gas phase and observed in solid-state. No significant change in the calculated bond angles of the compounds on comparing with the experimental values (c.f. Fig.

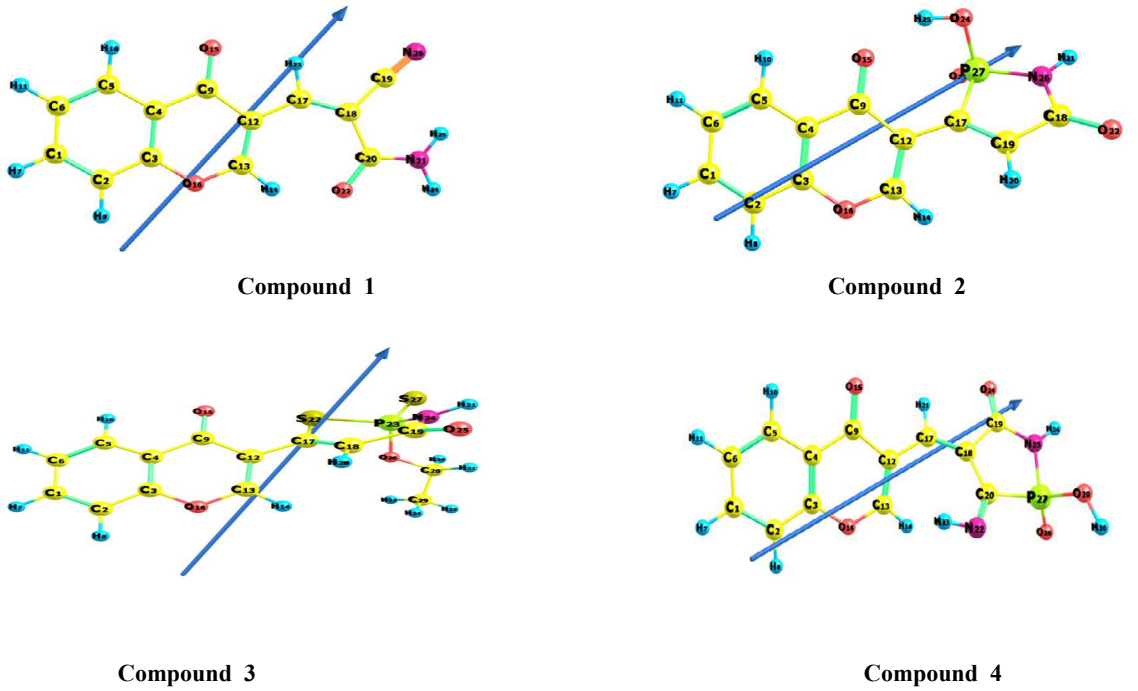


Fig. 2. The optimized structure, perspective view of dipole moment of the compounds 1-4 at B3LYP/6-311++G (d, p).

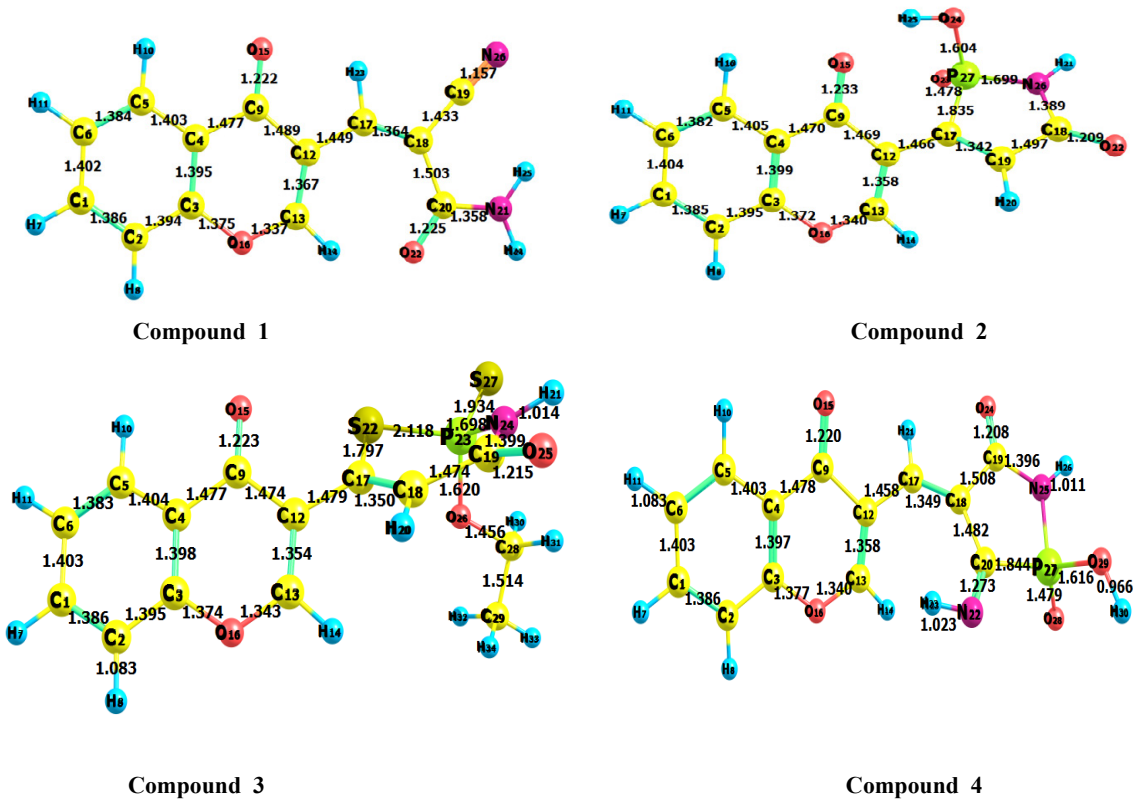


Fig. 3. The bond lengths of the compounds 1-4 at B3LYP/6-311++G (d,p).

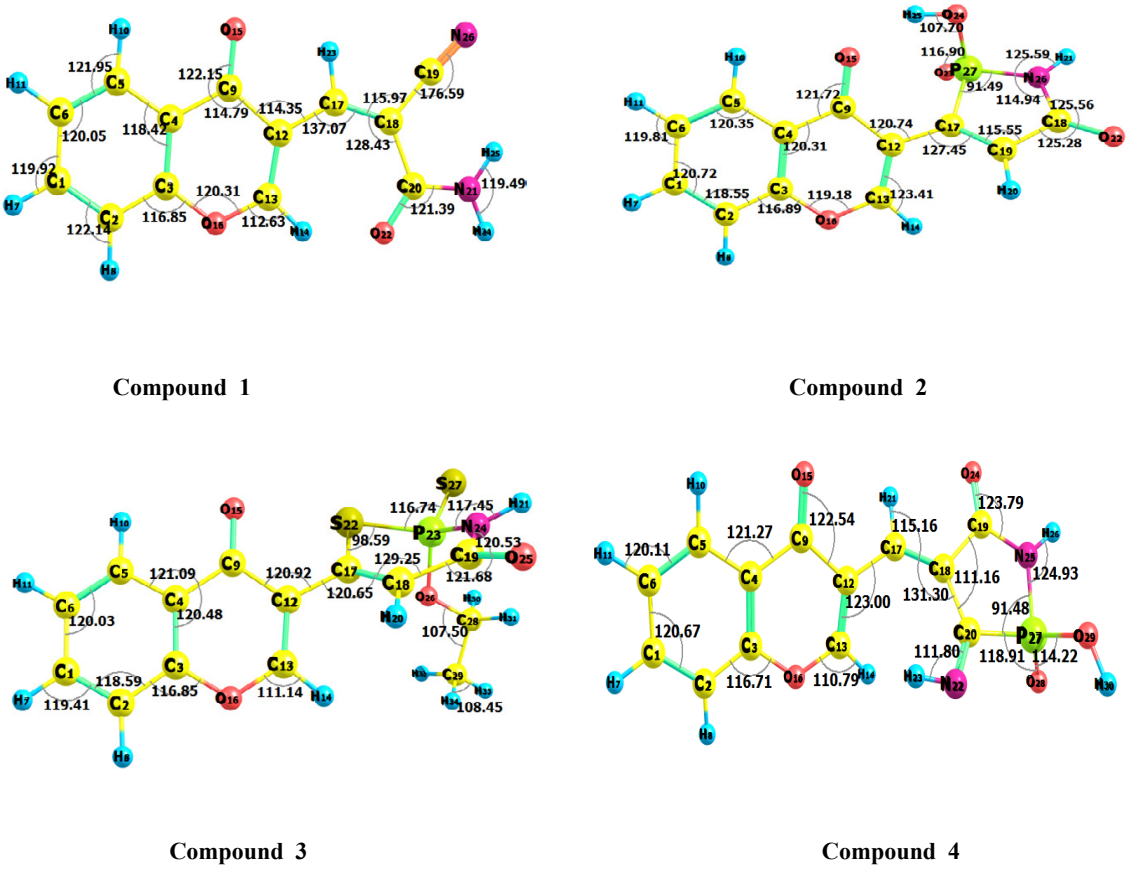


Fig. 4. The bond angles of the compounds 1-4 at B3LYP/6-311++G (d,p).

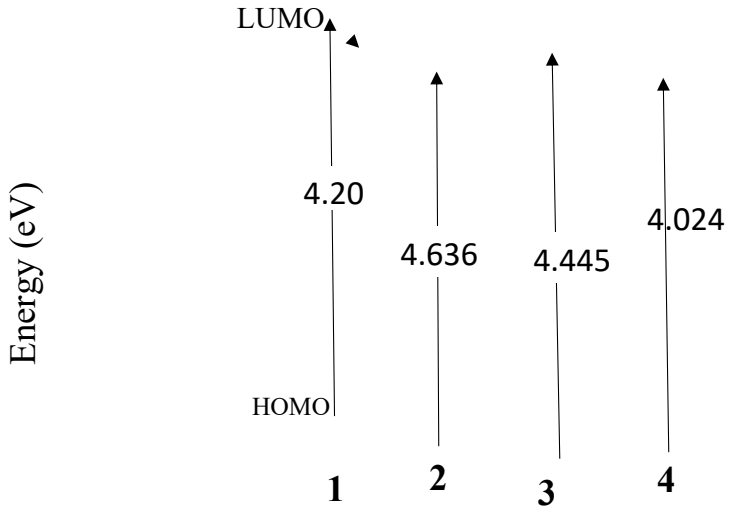


Fig. 5. Energy of HOMO, LUMO and energy gap of the studied compounds 1-4 at B3LYP/6-311++G (d, p) level of theory.

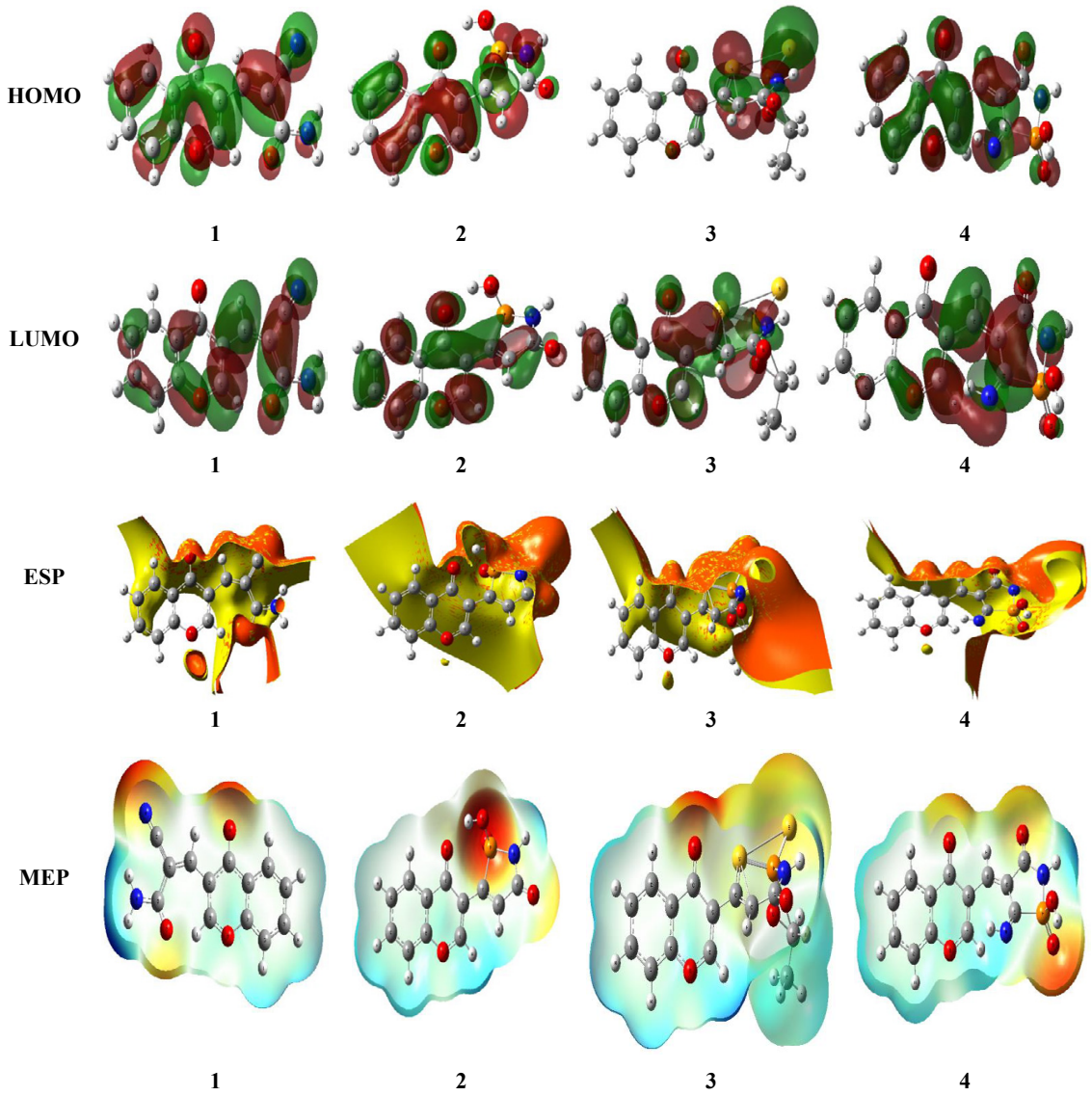


Fig. 6. HOMO, LUMO and Molecular surfaces of compounds 1-4 at B3LYP/6-311++G (d,p).

4). All the compounds are non-planner as reflected from their dihedral angles. In the parent compound **1**, the planarity changed by the presence of the phosphorus and sulfur atoms in diazaphosphinanes rings, by the range from 11° to 125°. So, there is no planarity for all compounds **2–4** as indicated from the dihedral angles (c.f. Table 1).

$E_{HOMO}$ of compound **1** which measures the donating property (oxidation power) is 6.90 eV (c.f. Table 3) and hence in the donating properties follows the order: **3 > 1 > 4 > 2** as shown in Table 3 and Fig. 5. However, $E_{LUMO}$ of **1** which measures the accepting property (reducing power) is 2.70 eV. The order of accepting properties follows **3, 2, 1, 4** as shown in Table 3 and Fig. 5. The bandgap, $E_{Gap}$, is the energy gap between $E_{HOMO}$ and $E_{LUMO}$, it signifies the facile electron transition from $E_{HOMO}$ to $E_{LUMO}$, i.e., the reactivity of molecules in the studied compounds **1-4** are governed by their chemical structures. The results in Table 3 and Fig. 5. shows that the computed reactivity in the gas phase of the studied compounds increases in the order: **4 > 1 > 3 > 2.** This indicates that the smaller the $E_{gap}$, the higher the reactivity of these compounds. Finally, the theoretically computed dipole moment, μ, for compound **1** which measures the

charge separation over the molecule is 5.07 D. The general trend of the dipole moment changes for the studied compounds follows the order **2 > 3 > 4 > 1** (c.f. Table 3) and the vector of the dipole moment is presented in Fig. 2.

The global descriptor study suggests all these are good electrophiles as the value of global electrophilicity is less. As far as global softness is concerned the compound **4** is the softest among all compounds **1-3** with a global softness value of 0.24851 eV. The absolute hardness is higher for compound **2** and it is 2.31812 eV. The ease of removal of an electron is governed by its chemical potential *V* (eV) and it is likewise identified with its electronegativity. A good electrophile is described by a higher value of global electrophilicity (ω) and the lower value of ω indicates good nucleophile. Our results suggest that compound **2** (ω = 1.71354 eV) has a higher value of ω, so it is most likely to accept electrons readily and would undergo nucleophilic attack easily. On the other hand, compound **1** (ω = 1.20616) has a lower electrophilicity indicating that it is a potent nucleophile or can lose easily. As the *V* value increases, the ability of a molecule to lose an electron increases.

*Natural Charge*

The natural population analysis [42] performed on the electronic structures of compounds **1-4** clearly describes the distribution of electrons in various sub-shells of their atomic orbits. The accumulation of charges on the individual atom has been presented in Table 2. In the case of our studied compounds **1-4**, the most negative centers are O15, O16, O22, N21, and N24-atoms. According to an electrostatic point of view of the molecule, these negative atoms tend to donate an electron. Whereas, the most electropositive atoms such as P27, S24, and S28 atoms, have been tend to accept an electron.

The natural population analysis [42] was performed on the electronic structures of compounds **1-4** are calculated by DFT/B3LYP method with 6-311++G (d, p) basis set in the gaseous phase are given in Table 2 and indicated by colors in Fig. 7, it is clearly described the distribution of electrons in various sub-shells of their atomic orbits. Natural atomic charges reveal that all the phosphor (P27) atoms have a net positive charge but compound **4** has a more positive charge (1.63626) than other compounds **1-3**. The high positive character is due to the attachment with a nitrogen atom and Sulphur atom. Amongst the nitrogen atom, the N24 atom has a more negative charge, and the value is -0.95589. The oxygen atom (O22) -0.65316 charge.

*Polarizability and hyperpolarizability*

The relationship between the molecular structure and NLO phenomena for the compounds **1-4** were calculated using DFT/B3LYP/6-311++G (d, p) has been also theoretically obtained [43]. Table 4 shows that the mean first-order hyperpolarizability $\langle\beta\rangle$ (Octa pole moment), total static dipole moment (μ), the mean polarizability (α) (Quadrupole moment), and the anisotropy of the polarizability (Δα), of the compounds **1-4**. The calculated high value of dipole moment was found to be 7.9444 D for compound **2** than the other compounds **1, 3** and **4** at B3LYP/6-311++G (d,p). Also, the calculated mean polarizability (α) for compound **3** is $41.47 \times 10^{-24}$ esu i.e., two times higher than PNA molecule, the order of increasing $\alpha$ with respect to PNA was showed in Table 4 that values of $\alpha$, β: compounds **2** and **4** are ~ 1.7 and 2 times higher than (PNA), whereas compounds **1** are ~ 1.5 times higher than the standard (PNA), respectively. In addition, the calculated mean first-order hyperpolarizability $\langle\beta\rangle$, of the compound **4** is $66.89 \times 10^{-30}$ esu and compound **3** is $57.23 \times 10^{-30}$ esu i.e., higher than PNA molecule (Table 4), while compounds **1, 2** are ~ 2, and 2.5 times higher than the reference, respectively. The obtained value indicates that the studied compounds **1-4** might be a promising NLO material. Due to the lack of any experimental NLO data about the examined compound, *p*-nitroaniline (PNA) that is one of the typical NLO structure [44-46] was chosen as reference material.

*Molecular electrostatic potential (MEP)*

The MEP and NAO plots for the studied compounds **1-4** are presented in Figs. 6-7. The MEP plots suggest that the chromone ring attached to the 1, 3, 2-thiazaphosphinin and 1,2-azaphospholidin the ring is highly susceptible to electrophilic aromatic substitution. In all the studied compounds **1-4**, the red part is situated at the NH group suggesting high reactivity towards basic reagents and caused by while the positive (blue) potential sites were around the hydrogen, and carbon atoms. Blue for electron deficient, (partially positive charge), red part (partially negative charge), light blue for (slightly electron-deficient region), yellow for (slightly electron rich region), green for neutral (zero potential)

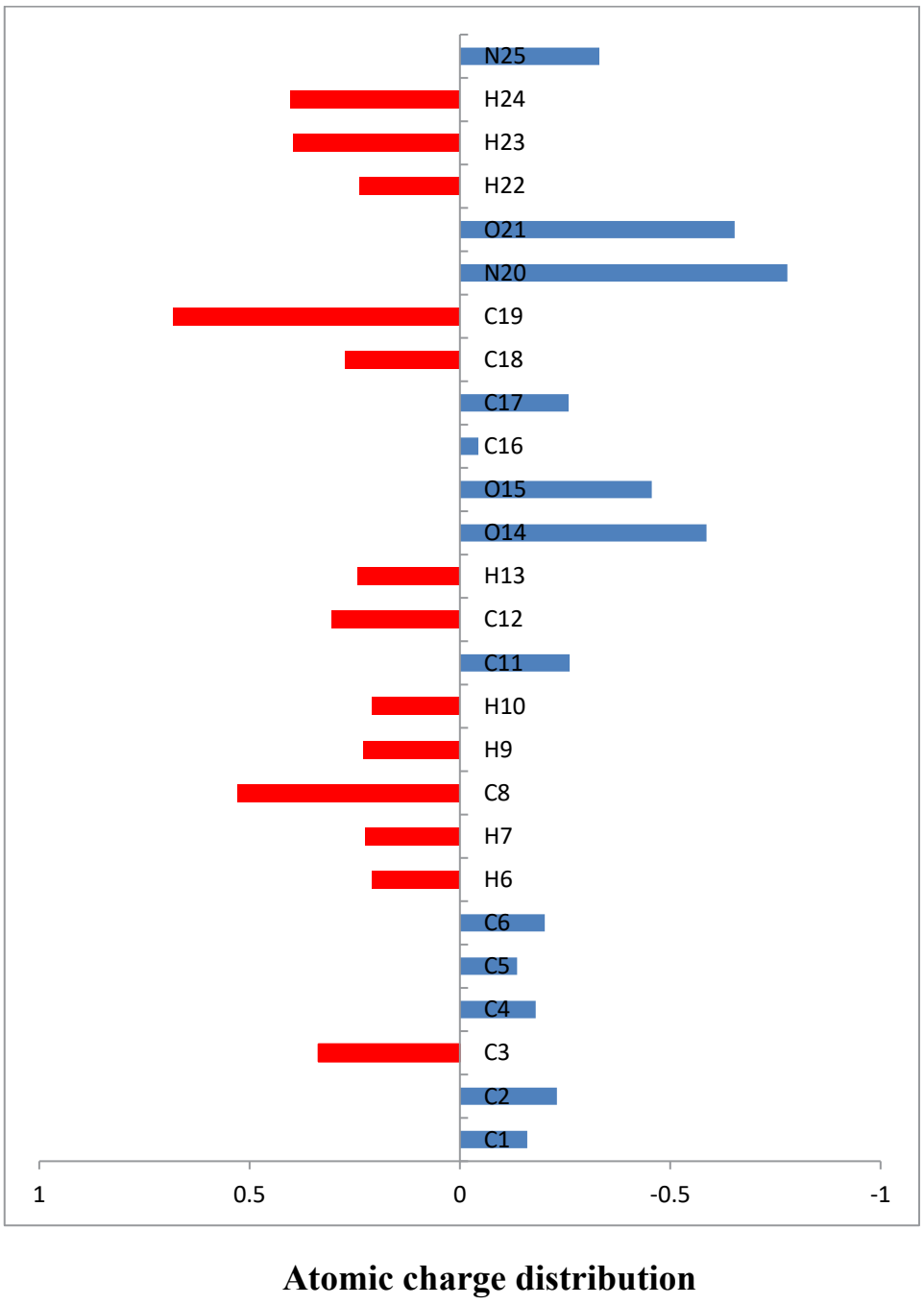


Fig. 7. Atomic charge distribution (au) for compound 1 at B3LYP/6-311++G (d,p) basis set.

respectively, [47-49].

*Electronic UV-Spectra*

Absorption energies (λ in nm), oscillator strength (f), and transitions of all studied compounds **1-4** have been computed at TD-DFT-CAM-B3LYP/6-311++G (d,p) level of theory for optimized geometries.

To understand the electronic transitions of the compounds **1-4**, the results of the TD-DFT were carried out in both the gas phase and in a polar solvent (methanol and butanol) and in non-polar solvent (dioxane, and toluene) for the low-intensity bands (Q-region) and high-intensity bands of the compounds **1-4**. The electronic spectra of compounds **1-4**, in methanol and butanol solvents, assignment of spectra is given in Figs. 8-15 and Tables 6-9. The charge density maps of the occupied and vacant MO, s considered in the transitions are presented in Fig. 16. The spectrum in (dioxane, and toluene) is composed of seven bands centered at 500 nm, 470 nm, 445 nm 375 nm, 325 280, and 255. Increasing solvent polarity ongoing from (dioxane, and toluene) to (methanol and butanol) cause's small changes in band positions indicating that the polarity of the excited and the ground state is of the same values, that is, solvent independent. The intensity is lowered in (methanol and butanol) and all bands are assigned to (π-π*) and (n-π*) transitions as reflected from their intensities (0-60000). The excited configurations considered in compounds **1-4**, are those which results from an electron excitation of the highest occupied molecular orbitals and the lowest vacant molecular orbitals. The correspondence between the theoretically computed and the experimentally observed transitions are satisfactory.

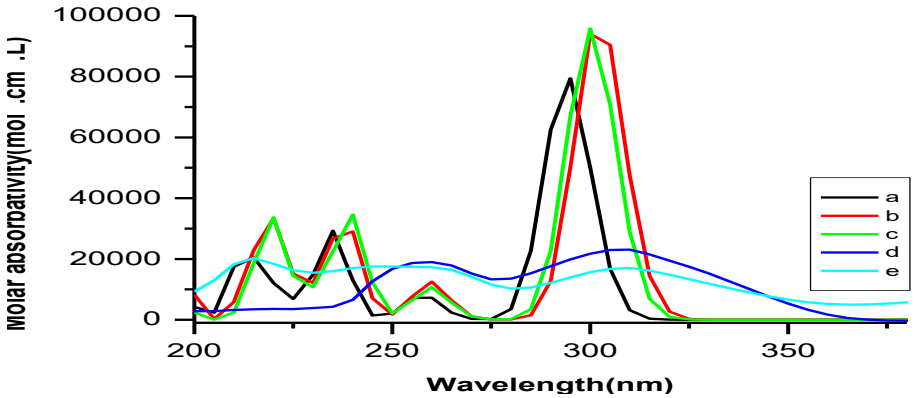


Fig. 8. Electronic absorption spectra of compound 1, (a) theoretical in gas phase, (b) theoretical in dioxane, (c) theoretical in methanol (d) experimental in dioxane, (e) experimental in methanol.

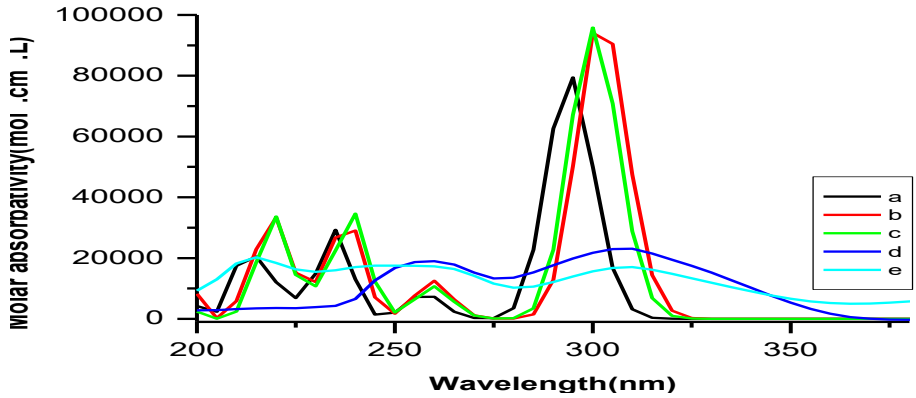


Fig. 9. Electronic absorption spectra of compound 1, (a) theoretical in gas phase, (b) theoretical in toluene, (c) theoretical in butanol (d) experimental in toluene, (e) experimental in butanol.

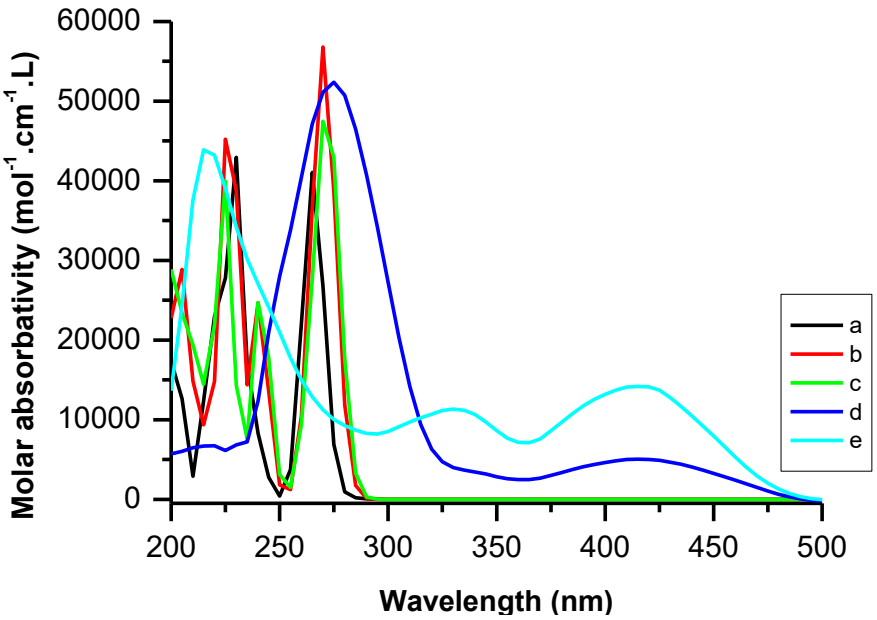


Fig. 10. Electronic absorption spectra of compound 2, (a) theoretical in gas phase, (b) theoretical in dioxane, (c) theoretical in methanol (d) experimental in dioxane, (e) experimental in methanol.

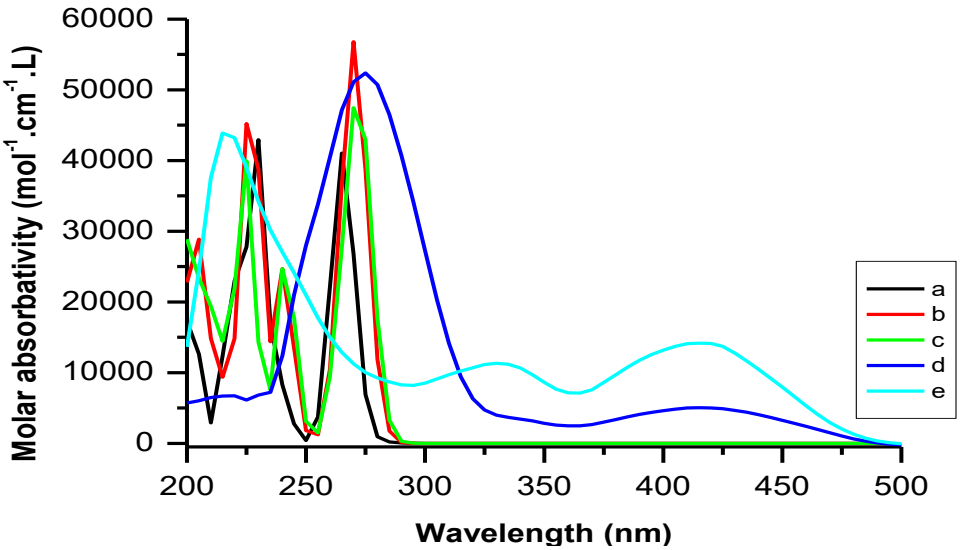


Fig. 11. Electronic absorption spectra of compound 2, (a) theoretical in gas phase, (b) theoretical in toluene, (c) theoretical in butanol (d) experimental in toluene, (e) experimental in butanol.

*Electronic absorption spectra of compound 1*

Figs. 8-9 and Table 6 present the experimental and theoretical electronic absorption spectra of **1** in (methanol and butanol) and (dioxane, and toluene). Increasing solvent polarity on going from (dioxane, and toluene) to (methanol and butanol) results in a blue shift, all bands are assigned to (π-π*) and (n-π*) transitions as reflected from their intensities (0-60000). To account for the experimentally observed UV Spectra of **1** in (dioxane, and toluene) and (methanol and butanol), it is essential to consider the theoretically calculated vertical transitions using TD-DFT-CAM-B3LYP/6-311++G (d, p) level. The experimental band at 430 nm (in dioxane, and toluene) is reproduced theoretically by using PCM (dioxane,

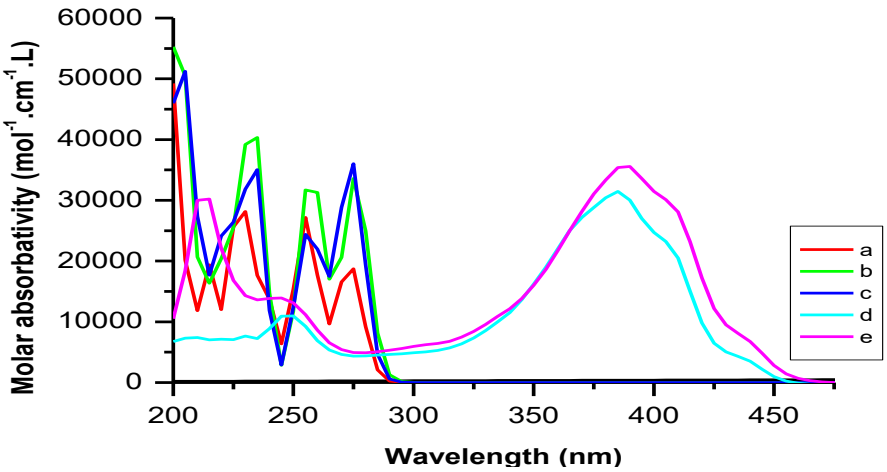


Fig. 12. Electronic absorption spectra of compound 3, (a) theoretical in gas phase, (b) theoretical in dioxane, (c) theoretical in methanol (d) experimental in dioxane, (e) experimental in methanol.

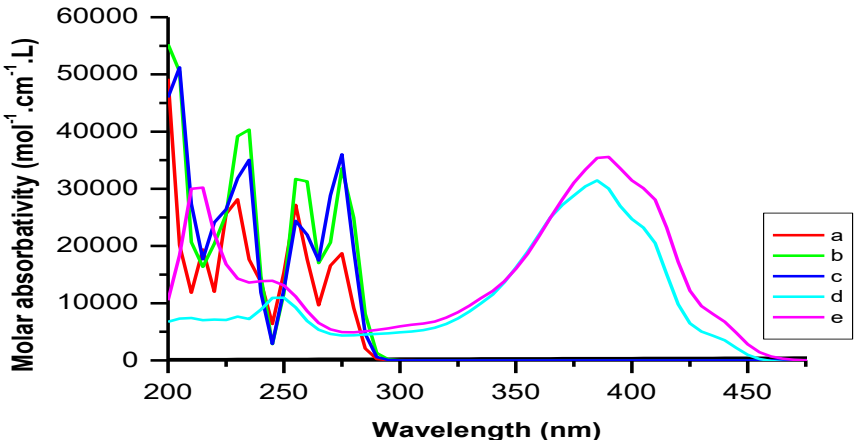


Fig.13. Electronic absorption spectra of compound 3, (a) theoretical in gas phase, (b) theoretical in toluene, (c) theoretical in butanol (d) experimental in toluene, (e) experimental in butanol.

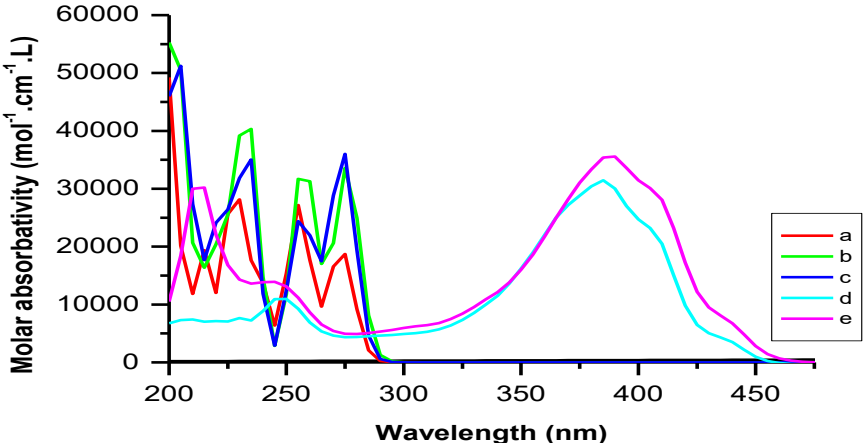


Fig.14. Electronic absorption spectra of compound 4, (a) theoretical in gas phase, (b) theoretical in dioxane, (c) theoretical in methanol (d) experimental in dioxane, (e) experimental in methanol.

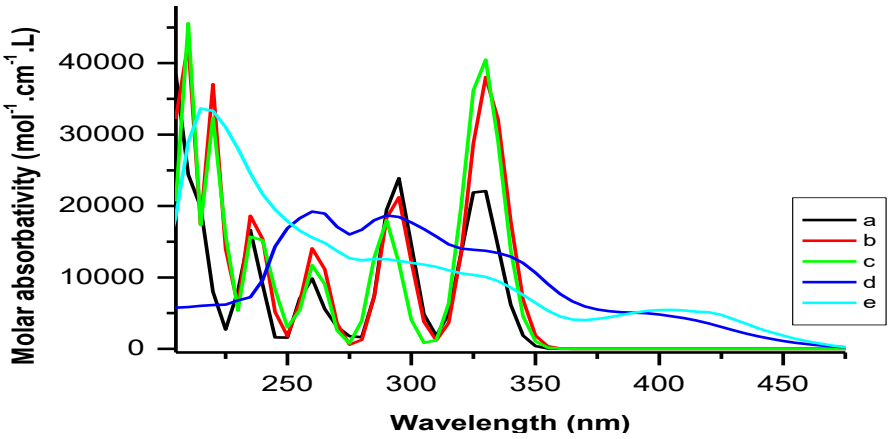


Fig.15. Electronic absorption spectra of compound 4, (a) theoretical in gas phase, (b) theoretical in toluene, (c) theoretical in butanol (d) experimental in toluene, (e) experimental in butanol.

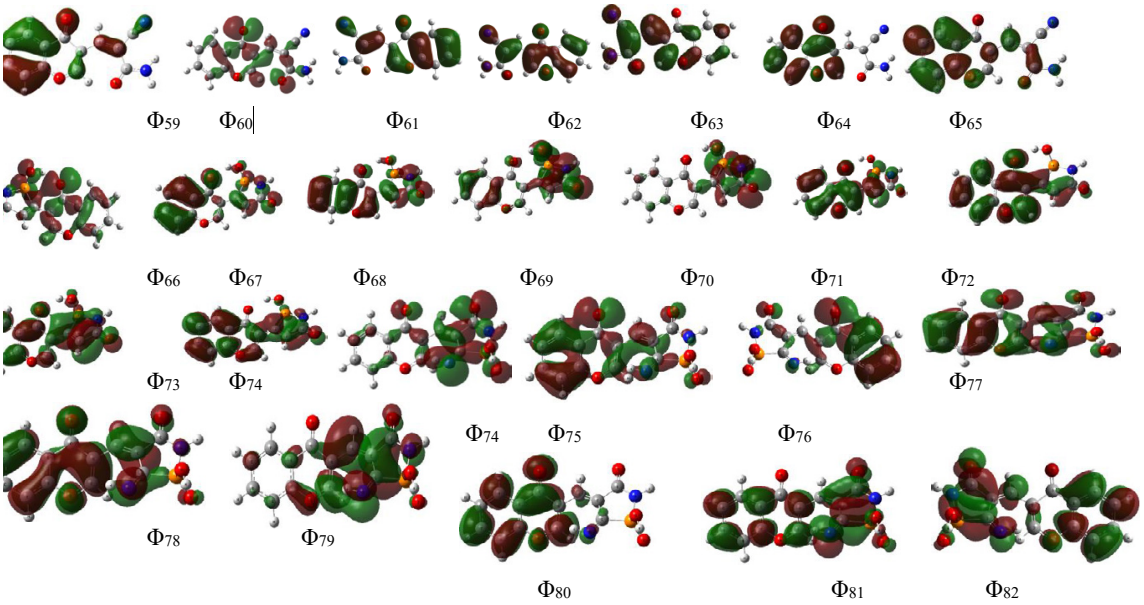


Fig. 16. Electron density contours of the studied compounds 1-4.

and toluene), at 450 (state 9) nm, and in the gas phase, at 420 nm as shown in Table 6. Moreover, in polar solvents (methanol and butanol), this same band appeared at (411 nm) respectively, where theoretical calculations in (methanol and butanol), reproduced this band at (425 nm) (state 11), as shown in Table 6. The electron density contours of molecular orbital's nature indicted by the electronic transition. The ten orbital's $\phi_{59\text{-}68}^{-1}$ involved in the theoretical transitions of compound **1**, is shown in Fig. 16, showed a delocalization of electron density, and charge transfer CT character. From the second state to eight states, the same desiccation as well as the first state (c.f. Figs. 8, 9, and Table 6). For comparison, Table 6 contains the theoretical and the experimental vertical excitation energies and the corresponding oscillator strengths for compound **1**.

The NBO analysis of the studied compounds **1-4** provides an efficient method for studying intra-and intermolecular bonding and provides a convenient basis for investigating charge transfer or conjugative interactions in molecular systems. Table 5 presents the second-order perturbation

energies of most interacting NBOs of **1-4** and the most important interaction between filled (donor) Lewis's type NBOs and empty (acceptor) non-Lewis NBOs. The charge density maps of HOMO and LUMO for **1-4** are presented in Fig.16. The results of NBO analysis of compound **1** tabulated in Table 5 indicate that there is a strong hyper conjugative interactions $\pi^*C_3$-$C_4$ → $\pi^*C_5$-$C_6$, $\pi^*C_{20}$-$O_{22}$ → $\pi^*C_{17}$-$C_{18}$, LP (1) $N_{21}$ → $\pi^*C_{20}$-$O_{22}$, and LP (2) $O_{16}$ → $\sigma^*C_{12}$-$C_{13}$, for **1** is 176.33, 106.80, 64.83, and 36.17 kcal/mol, respectively. The C–O π orbital and quinoline ring interact equally well with the chromone ring. In fact, its interaction with the chromone ring is greater. Furthermore, the lone pair orbital of the oxygen and nitrogen atoms enjoys hyperconjugation with the C20–O22, and C1–C2 π* orbital. It is surprising to notice a decrease in the population of the NBO C1–C2, and C3–C4 reflecting a charge transfer away from the chromone ring. In conclusion, **1** enjoys the linear conjugation that is responsible for the observed spectrum. No specific part of the molecule manifests itself in the observed spectrum.

*Electronic absorption spectra of compound 2-4*

The gas-phase calculation gave a wavelength at 460 nm. Moreover, in polar solvents (methanol and butanol), this same band appeared at (450 nm) respectively, where theoretical calculations in (methanol and butanol), reproduced this band at (480 nm) (state 11), while in non-polar solvents (dioxane, and toluene) centered at (450 nm), in compounds **2-4,** this band is predicted theoretically at (500 nm) (state 9), respectively, it is very good agreement with the experiment. As shown in Tables 7-9. The electron density contours of molecular orbital's nature indicted by the electronic transition. The ten orbital's $\phi_{65\text{-}76}^{-1}$, $\phi_{85\text{-}97}^{-1}$, and $\phi_{95\text{-}106}^{-1}$, respectively involved in the theoretical transitions of compounds **2-4**, is shown in Fig. 15, showed a delocalization of electron density, and charge transfer CT character. From the second state to eight states, the same desiccation as well as the first state (c.f. Figs. 10-15 and Tables 7-9). These absorption bands in the visible region are typical n-π*, π–π* transitions. The absorption band that corresponds to the maximum absorption of the compounds **2-4**, is blue and red-shifted by 3 -4 nm under the effect of solvent. For comparison, Tables 7-9 contains the theoretical and the experimental vertical excitation energies and the corresponding oscillator strengths for compounds **2-4**.

Table 5 presented the second-order perturbation energies of most interacting NBOs of **1-4** and the most important interaction between filled (donor) Lewis's type NBOs and empty (acceptor) non-Lewis NBOs. Fig. 6 presented the charge density maps of HOMO and LUMO for **1-4**. NBO analysis of compound **2** in Table 5 indicated that it retained the extended conjugation of **1** as revealed by the interaction of C–O NBOs with those of chromone ring. Furthermore, the oxygen lone pair orbital and nitrogen atoms enjoyed hyperconjugation with the $C_3$–$C_4$, $C_{18}$–$O_{22}$, and $C_{18}$–$N_{26}$ π* orbital. It was surprising to notice a decrease in the population of the NBO $O_{24}$– $P_{27}$, and $C_3$–$C_4$ reflecting a charge transfer away from the chromone ring. There was a strong hyper conjugative interaction in Compound **3,** $\pi^*C_3$-$C_4$ → $\pi^*C_5$-$C_6$, LP (1) $N_{24}$ → $\pi^*C_{19}$-$O_{25}$ and LP (2) $O_{16}$ → $\pi^*C_{12}$-$C_{13}$, for **3** is 153.39, 42.82, and 33.08 kcal/mol, respectively. Furthermore, the lone pair orbital of the oxygen and nitrogen atoms enjoyed hyperconjugation with the $C_{12}$-$C_{13}$, and $C_{19}$-$O_{25}$ π*-orbital. The population of the NBO $P_{23}$–$N_{24}$, $P_{23}$–$O_{26}$, and $C_3$–$C_4$ decrease surprising and reflecting a charge transfer away from the chromone ring. This was also evident in the case of the population of the oxygen lone orbital LP (1) $N_{24}$. The results of compound **4** of NBO analysis tabulated in Table 5 indicated that there was a strong hyper conjugative interaction $\pi^*C_3$-$C_4$ → $\pi^*C_5$-$C_6$, $\pi^*C_{12}$-$C_{13}$ → $\pi^*C_9$-$O_{15}$, and LP (1) $N_{25}$ → $\pi^*C_{19}$-$O_{24}$, for **4** was 152.68, 110.96, and 50.24 kcal/mol, respectively. There is the extended conjugation of **1** with compound **4** as revealed by the interaction of C–O NBOs with those of chromone ring. It a decrease in the population of the NBO $C_3$–$C_4$, $C_9$–$O_{15}$, $C_{17}$–$C_{18,}$ and $C_{20}$–$P_{27}$ reflecting a charge transfer away from the chromone ring can be surprised. This was also evident in the case of the population of the oxygen lone orbital LP (1) $N_{25}$.

*Optical band gap of the presented structures*

The main experimental optical parameter of the presented structures is the energy gap, Eg which can be obtained for the direct type of transition by using the following Eq. [4] [50]:

$(\alpha E)^2 = A (E - E_g)$

Where, E is the incident photon energy and A is a constant of incident photon energy. As observed from Figs. 17-20 that the best fit of the most feasible transition supports the direct band transition. The values of $E_g$ for every structure that

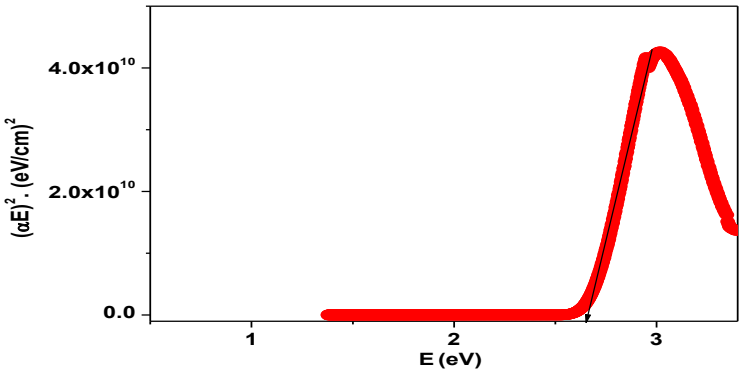


Fig. 17. Energy gap of Compound 1.

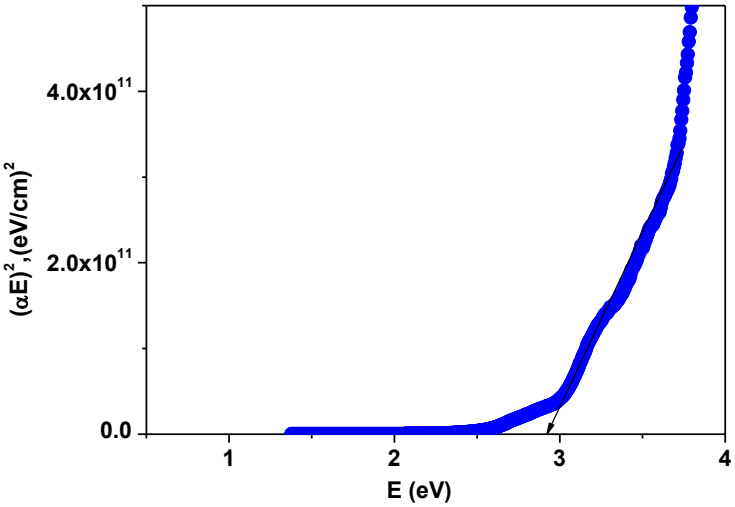


Fig. 18. Energy gap of Compound 2.

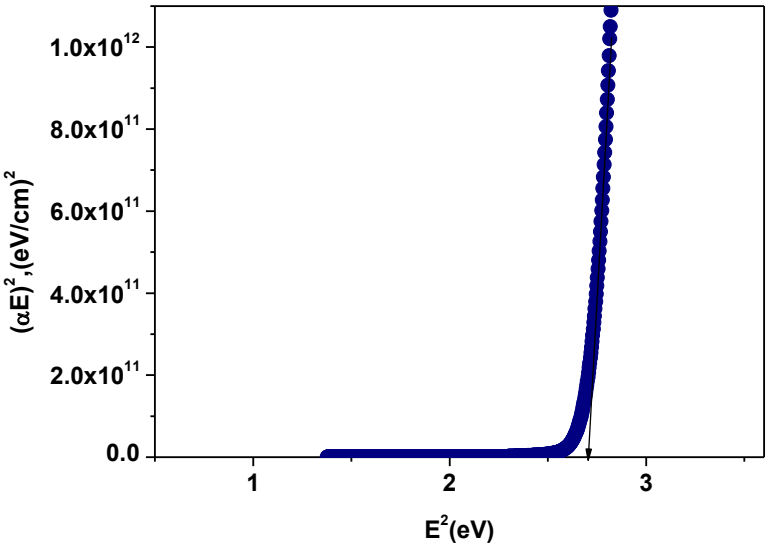


Fig. 19. Energy gap of Compound 3.

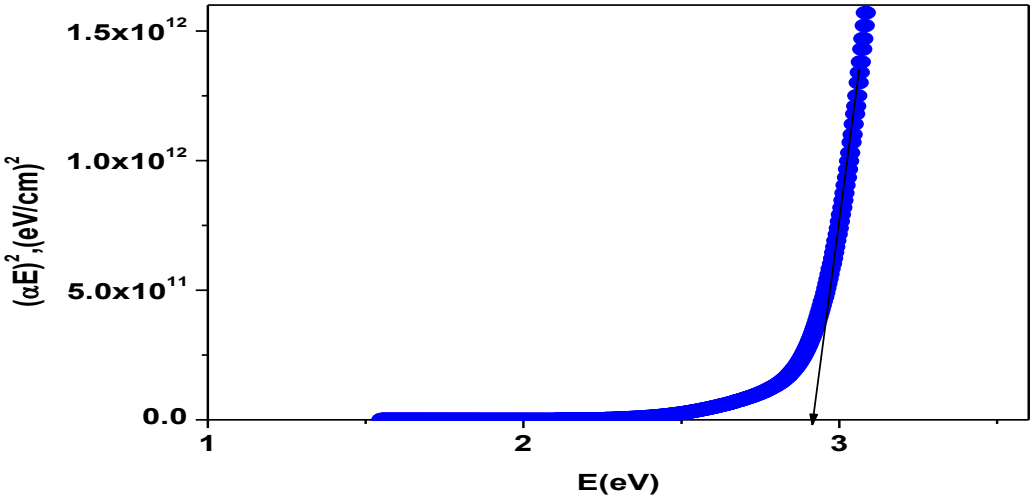


Fig. 20. Energy gap of Compound 4.

resulting from [(α E)$^2$ vs (E)] plots can be extracted from extrapolation of linear parts of the curve for each case to (α hν)$^2$ = 0 as shown in the Figs. 17-20. The obtained $E_g$ values of the compounds **1-4** follow that, 2.84, 2.55, 2.60 and to 2.82eV, respectively.

## CONCLUSION

In summary, we have explored various facets of the electronic structure of 1, 2, 3-thiazaphosphinine and 1, 2-azaphospholes bearing a chromone ring for all studied compounds **1–4**, were investigated theoretically by using the DFT method at B3LYP/6-311++G (d, p) and TD-DFT at CAM/B3LYP/6-311++G (d, p) level theory. The results of our investigation are summarized below:

1. The geometry of all compounds **1–4** is optimized B3LYP/6-311++G (d, p) basis set. All these molecules possess C1 point group symmetry.

2. For a detailed structural analysis, the optimized geometrical parameters like bond lengths and bond angles have been discussed, also, all compounds were found to be non-planar structure indicated by dihedral angle.

3. Frontier molecular orbital analysis of all compounds **1–4** has been computed and the results indicate that compound **4** had the lowest $E_{HOMO}$, $E_{LUMO}$, and $E_{gap}$ indicating the highest reactivity amongst all compounds. This means that the inevitable charge transfer is easier in compound **4** than other compounds.

4. Various quantum chemical parameters have been computed to analyze the chemical nature of the molecules.

5. The neutral atomic charges for all compounds **1–4** which indicated the electronic charge distribution has been discussed.

6. The calculated dipole moment and first order hyperpolarizability results indicated that the molecule had a reasonably good non-linear optical behavior.

7. The molecular electrostatic potential (MEP) surfaces are plotted to point out the electrophilic and nucleophilic reactivity sites.

8. Absorption energies (λ in nm) spectra of the compounds **1–4** have been computed at TD-DFT-CAM/B3LYP/6-311++G (d, p) level of theory. All the observed bands can be assigned to (n-π*, π–π*) transitions as reflected from their intensities. The correspondence between the theoretically computed and the experimentally observed transitions are satisfactory. The solvent dependence of the observed bands can be attributed to the charge in the dipole moments of the ground and excited states.

9. The NBO analysis of compounds **1–4** indicated the intermolecular charge transfer between the bonding and anti-bonding orbitals.

10. Band gaps optical were extracted from the photon energy dependence on absorption coefficient at the band edges and found to be 2.84, 2.55, 2.60 and 2.82eV, respectively.

In this way, we can conclude that the information furnished in this research could provide a ladder for the development of further research in the respective fields.

## CONFLICT OF INTEREST

Authors have no conflict of interest.

## REFERENCES


[1] Hassanin N. M., Ali T. E., El-Shaaer H. M., Hassan M. M., (2019), Reaction of 2-Imino-2H chromene3carboxamide with Phosphorus isothiocyanates: First synthesis of novel chromeno [2, 3-d ] pyrimidinyl and Bis(chromeno [2, 3-d ] pyrimidinyl) phosphines and Chromeno[2', 3' : 4, 5] pyrimido[2, 1d ][1, 3, 5, 2] triazaphosphinine. *J. Heterocycl. Chem.* 56: 1646-1650.

[2] Guanghui An, Cole S., Guigen Li, (2015), N-Phosphonyl/ phosphinyl imines and group-assisted purification (GAP) chemistry/technology. *J. Org. Biomol. Chem.* 13: 1600-1617.

[3] Long N., Cai X. J., Song B. A., Yang S., Chen Z., Bhadury P. S., Lu D. Y., Jin L. H., Xue W., (2008), Synthesis and antiviral activities of cyanoacrylate derivatives containing an alpha-aminophosphonate moiety. *J. Agric. Food.* 56: 5242-5246.

[4] Wang Q., Zhu M., Zhu R., Lu L., Yuan C., Xing S., Fu X., Mei Y., Hang Q., (2012), Eur Exploration of α-Aminophosphonate N-derivatives as novel, potent and selective inhibitors of protein tyrosine phosphatases. *J. Med. Chem.* 49: 354-364.

[5] Dake S., Raut, A., Kharat D. S., Mhaske K. R., Deshmukh R. S., Pawar S. M., (2011), Synthesis of novel a-Aminophosphonate derivatives, biological evaluation as potent antiproliferative agents and molecular docking. Bioorg. *Med. Chem. Lett.* 21: 2527-2532.

[6] Abdou W. M., Barghash R. F., Bekheit M. S., (2012), One-pot three-component synthesis of novel diethyl ((2-oxo-1, 2-dihydroquinolin-3-yl) (arylamino) methyl) phosphonate as potential anticancer agents. *J. Arch. Pharm. Chem. Life Sci.* 345: 884-895.

[7] Akbas H., Okumus A., Kılıc Z., Hokelek T., Celik Z. B., (2013), Phosphorus-nitrogen compounds part 27. syntheses, structural characterizations, antimicrobial and cytotoxic activities, and DNA interactions of new phosphazenes bearing secondary amino and pendant (4-fluorobenzyl) spiro groups. *Eur. J. Med. Chem.* 70: 294-307.

[8] Chang C., Wu C., Kuo S., Wang J., Teng C., (2002), Natural products as sources of new drugs from 1981 to 2014. *Chin. Pharm. J.* 54: 127-138.

[9] Nohara A., Ishiguro T., Ukawa K., Sugihara H., Maki Y., Sanno Y., (1985), Studies on antianaphylactic agents, synthesis of antiallergic 5-Oxo-5H-[1]benzopyrano[2, 3-b] pyridines. *J. Med. Chem.* 28: 559-568.

[10] Lee S. K., Chae S. M., Yi K. Y., Kim N. J., Oh C. H., (2005), Synthesis and photoelectrical characterizations of ECPPQT for optoelectronic application. *Bull. Korean Chem. Soc.* 26: 619-629.

[11] Ukawa K., Ishiguro T., Kurik H., Nohara A., (1985), ChemInform abstract: Synthesis of heteroannulated chromeno[2, 3-b] pyridines: DBU catalyzed reactions of 2-Amino-6-methylchromone-3-carboxaldehyde with some heterocyclic enols and enamines. *Chem. Pharm. Bull.* 33: 4432-4442.

[12] Huang W., Ding Y., Miao Y., Liu M.-Z., Li Y., Yang G.-F., (2009), Cytotoxic activity evaluation and QSAR study of chromene-based chalcones. *Eur. J. Med. Chem.* 44: 3687-3696.

[13] Larget R., Lockhart B., Renard P., Largeron M., (2000), Amino and nitro derivatives of 5, 7-dimethoxyflavone from Kaempferia parviflora and cytotoxicity against KB cell line. Bioorg. *Med. Chem. Lett.* 10: 835-838.

[14] Ungwitayatorn J., Samee W., (2004), Pimthon, In vitro cytotoxicity of hydrazones, pyrazoles, pyrazolo-pyrimidines, and pyrazolo-pyridine synthesized from 6-substituted 3-formylchromones. *J. Mol. Struct.* 99: 689-699.

[15] Ishakava T., Oku Y., Tanaka T., Kumamoto T., (1999), Yttrium oxide (Y2O3): Efficient and green catalysis for the synthesis of chromeno [2, 3-b]quinolinedione. *Tetrahed. Lett.* 40: 3777-3787.

[16] Göker H., Boykin D. W., Yıldız S., (2005), Facile ionic liquid-mediated, microwave assisted green synthesis, and antioxidant studies of novel indolin-2-one annulated spirochromanone conjugates. *Bioorg. Med. Chem.* 13: 1707-1718.

[17] Deng Y., Lee J. P., Ramamonjy, M. T., Synder J. K., Des Etages S. A., Kanada D., Synder M. P., Turner C. J., (2000), Synthesis and characterization of new chromeno[2, 3-b] pyridines via the Friedländer reactions of 8-allyl-2-amino-4-oxo-4H-chromene-3-carboxaldehyde. *J. Nat. Prod.* 63: 1082-1091.

[18] Pietta P. J., (2000), Flavonoids as antioxidants. *J. Nat. Prod.* 63: 1035-1042.

[19] Mazzei M., Sottofattori E., Dondero R., Ibrahim M., Melloni E., Michetti M., (1999), Synthesis of some novel heteroannelated chromones by basic rearrangement of 6-methylchromone-3-carbonitrile. *Farmaco.* 53: 452-462.

[20] Ali T. E., Hassan M. M., (2018), Facile synthesis of novel 6-methyl-5-phenyl-2-sulfido-1, 2, 3, 5-tetrahydro-4H[1, 2] oxazolo [4', 5' : 5, 6] pyrano[2, 3-d][1, 3, 2] diazaphosphinines. *Res. Chem. Intermed.* 44: 173-181.

[21] Mirali M., Jafariazar Z., Mirzaei M., (2021), Loading tacrine alzheimer's drug at the Carbon nanotube: DFT approach. *Lab-in-Silico.* 2: 3-8.

[22] Mirzaei M., (2020), Science and engineering in silico. *Adv. J. Sci. Eng.* 1: 1-2.

[23] Faramarzi R., Falahati M., Mirzaei M., (2020), Interactions of fluorouracil by CNT and BNNT: DFT analyses. *Adv. J. Sci. Eng.* 1: 62-66.

[24] Kun H., Osman Murat O., Mirzaei M., (2020), Lithium adsorption at the C20 fullerene-like cage: DFT approach. *Adv. J. Sci. Eng.* 1: 74-79.

[25] Frisch M., Trucks J. G. W., Schlegel H. B., Scuseria G. E., (2009), Gaussian, Inc., Wallingford CT.

[26] Becke A. D., (1993), A new mixing of Hartree–Fock and local density-functional theories. *J. Chem. Phys.* 98: 1372-1376.

[27] Lee C., Yang W., Parr R. G., (1988), Development of the Colle-Salvetti correlation-energy formula into a functional of the electron density. *Phys. Rev. B. Condens. Matter.* 37: 785-789.

[28] Stefanov B., Liu G., Liashenko A., Piskorz P., Komaromi I., Martin R. L., Fox D. J., Keith T., A. Al-Laham M., Peng C. Y., Nanayakkara A., Challacombe M., Gill P. M. W., Johnson B., Chen W., Wong M. W., Gonzalez C., Pople J. A., (2003), Gaussian, Inc., Pittsburgh PA.

[29] Dennington R., Keith T., Millam J. Semichem Inc., (2009), GaussView, Version 5, Shawnee Mission KS.

[30] Miehlich B., Savin A., Stolt H., Preuss H., (1989), Results obtained with the correlation energy density functional of becke and lee, yang and parr. *Chem. Phys. Lett.* 157: 200-206.

[31] Avci D., (2011), Second and third-order nonlinear

optical properties and molecular parameters of azo chromophores: Semiempirical analysis. *Spectrochim. Acta A.* 82: 37-43.

[32] Avci D., Başoğlu A., Atalay Y., (2010), Ab initio HF and DFT calculations on an organic non-linear optical material. *Struct. Chem.* 21: 213-219.

[33] Avci D., Cömert H., Atalay Y., (2008), Ab initio hartree-fock calculations on linear and second-order nonlinear optical properties of new acridine-benzothiazolylamine chromophores. *J. Mol. Mod.* 14: 161-169.

[34] Pearson R. G., (1986), Absolute electronegativity and hardness correlated with molecular orbital theory. *Proc. Nat. Acad. Sci.* 83: 8440-8441.

[35] Chandra A. K., Uchimara T., (2001), Hardness Profile: A critical study. *J. Phys. Chem. A.* 105: 3578-3582.

[36] Matecki J. G., (2010), Phosphoinositides: Tiny lipids with giant impact on cell regulation. *Trans. Met. Chem.* 35: 801-811.

[37] Yanai T., Tew D., Handy N., (2004), A new hybrid exchange–correlation functional was using the Coulomb-attenuating method (CAM-B3LYP). *Chem. Phys. Lett.* 393: 51-57.

[38] Chocholoušová J., Špirko V., Hobza P., (2004), First local minimum of the formic acid dimer exhibits simultaneously red-shifted O–H…O and improper blue-shifted C–H…O hydrogen bonds. *Phys. Chem.* 6: 37-41.

[39] Szafran M., Komasa A., Bartoszak-Adamska E., (2007), Crystal and molecular structure of 4-carboxypiperidinium chloride (4-piperidinecarboxylic acid hydrochloride). *J. Mol. Struct.* 827: 101-107.

[40] Macoonald J. N., Mackay S. A., Tyler J. K., Cox A. P., Ewart I. C., (1981), Microwave spectra, structures and dipole moments of 4H-pyran-4-one and its sulphur analogues. *J. Chem. Soc. Farady. Trans. II.* 77: 79-99.

[41] Sajan D. Y., Erdogdu R., Reshmy O., Dereli K., Thomas K., Hubert I., (2011), Systematic ab initio gradient calculation of molecular geometries, force constants, and dipole moment derivatives. Spectrochim. *Acta Part A.* 82: 118-128.

[42] Reed A. R., Weinstock R. B., Weinhold F., (1985), Natural population analysis. *J. Chem. Phys.* 83: 735-742.

[43] Natorajan S., Shanmugam G., Martin S. A., (2008), Nonlinear optical properties of organic molecules and crystals. *Cryst. Res. Technal.* 43: 561-569.

[44] Cheng L. T., Tam W., Stevenson S. H., Meredith G. R., Rikken G., Marder S. R., (1991), Electric field induced second harmonic generation with and without fringes. *J. Phys. Chem.* 95: 10631-10640.

[45] Kaatz P., Donley E. A., Shelton D. P., (1998), Analysis of nonlinear optical properties in donor–acceptor materials. *J. Chem. Phys.* 108: 849-858.

[46] Gnanasambandan T., Gunasekaran S., Seshadri S., (2014), Experimental and theoretical study of p-nitroacetanilide. *Spectrochim. Acta Part A: Molec. Biomolecul. Spec.* 117: 557-567.

[47] Sscrocco E., Tomasi J., (1978), Electronic molecular structure, reactivity and intermolecular forces: An euristic interpretation by means of electrostatic molecular potentials. *Adv. Quant.Chem.* 11: 115-193.

[48] Politzer P., Murray J. S., (2002), The fundamental nature and role of the electrostatic potential in atoms and molecules. *Theor. Chem. Acc.* 108: 134-142.

[49] Sajan D., Joseph L., Vijayan N., Karabacak M., (2011), Natural bond orbital analysis, electronic structure, non-linear properties and vibrational spectral analysis of l-histidinium bromide monohydrate: A density functional theory. *Spectrochim. Acta A.* 81: 85-98.

[50] Hemalatha K. S. K., Rukmani N., Suriyamurthy B. M., (2014), Nagabhushana, scheelite-type MWO4 (M = Ca, Sr, and Ba) nanophosphors: Facile synthesis, structural characterization, photoluminescence, and photocatalytic properties. *Mater. Res. Bull.* 51: 438-448.